第32卷第12期 焊 接 学 报 Vol. 32 No. 12
2011年12月 TRANSACTIONS OF THE CHINA WELDING INSTITUTION December 2011

附加屏蔽气体的大气等离子喷涂对热障涂层性能影响

魏 琪，李 辉，李 红，张林伟
（北京工业大学 材料科学与工程学院，北京 100124）

魏 琪

摘 要：对比研究了附加屏蔽气体的大气等离子喷涂和普通大气等离子喷涂对热障涂层组织结构和性能的影响. 结果表明，附加屏蔽气体的大气等离子喷涂粘结层表面未熔或半熔粒子较少，涂层中氧化物夹杂和孔隙率降低，热障涂层在1 080 ℃下具有更好的抗氧化性能. 附加屏蔽气体的大气等离子喷涂的热障涂层具有更好的抗氧化性能的原因，在于外加保护气氛减轻了喷涂过程中粒子和涂层的氧化，粘结层中Al元素含量更高，氧化初期粘结层表面优先形成致密的具有保护作用的Al_2O_3薄膜，使得界面热生长氧化物的生长速度减慢.

关键词：等离子喷涂；热障涂层；抗氧化性能
中图分类号：TG115.28 **文献标识码**：A **文章编号**：0253－360X(2011)12－0051－04

0 序 言

随着航空航天事业的发展和燃气轮机的广泛应用，对材料的高温性能要求越来越高. 如燃气轮机的热端部件，其承受温度高达1 100～1 400 ℃，已超过耐高温材料的极限使用温度. 热障涂层(thermal barrier coatings，TBCs)能降低工件的受热温度，延长零件寿命，提高热机热效率，因此热障涂层的制备和应用已成为一个重要的研究方向[1].

实际应用的热障涂层大多为金属粘结层和陶瓷面层的双层结构，其中MCrAlY合金粘结层和氧化钇稳定的氧化锆(YSZ)面层应用最为广泛. 在各种热障涂层制备方法中，大气等离子喷涂(atmospheric plasma spraying，APS)由于具有沉积效率高，成本低，隔热性能好的特点而应用最为广泛. 但是APS喷涂时金属粒子容易氧化[2]，这对涂层的性能将产生较大的影响，易造成陶瓷面层的剥落[3,4]. 因此如何提高APS热障涂层的性能一直是研究的热点[1,4]. 文中以NiCrCoAlY粘接层ZrO_2-8%Y_2O_3面层的热障涂层为对象，研究了附加屏蔽气体的大气等离子喷涂(shroud plasma spraying，SPS)和APS对热障涂层组织结构和性能的影响.

收稿日期：2011－01－22
基金项目：北京市教委科技发展项目(KM200610005026，JP009012200803)；
北京工业大学博士启动基金(52009999200701)

1 试验方法

喷涂基体材料为Haynes230镍基高温合金，喷涂前预先进行喷砂粗化处理，然后置于丙酮中进行超声波清洗. 喷涂材料为粒度44～104 μm的NiCrCoAlY粉(元素含量为C＜0.7%，O 0.95%，Y_2O_3 1.5%～2.0%，Co 3%～5%，Al 4%～6%，Cr 14%～16%，其余为Ni)(质量分数)和粒度为44～74 μm的ZrO_2-8%Y_2O_3粉. 采用装备有NX100型Motoman机器人的Sluzer Metco 9M喷涂设备，送粉器为Metco 5MP，喷涂工艺参数为：电压75 V，电流500 A，主气流量(Ar)45 L/min，辅气流量(H_2)10 L/min，送粉率35 g/min. 附加屏蔽气罩中氩气流量为65 L/min. 用光学显微镜观察涂层的组织结构，并用Matlab图像分析软件测定涂层孔隙率和热生长氧化物的厚度. 采用FEI Quanta 200扫描电镜－能谱仪(SEM)进行涂层表面与截面的形貌观察和点成分分析. 用BRUKER D8 Advance X射线衍射仪(XRD)对涂层进行物相分析. 在1 080 ℃静态空气氛围下测量涂层试样的氧化增重.

2 试验结果与讨论

2.1 粘结层微观组织结构

图1，图2为APS和SPS粘结层表面和截面形

貌. 可以看出 SPS 粘结层表面较 APS 粘结层细密，夹杂物少. 这是因为减少了周围空气的卷入和对焰流的扰动，使粒子的速度和温度有所提高[5]，改善了粒子的氧化和熔化情况[6]，使涂层表面未熔或半熔粒子减少，表面粗糙度下降，氧化物夹杂减少.

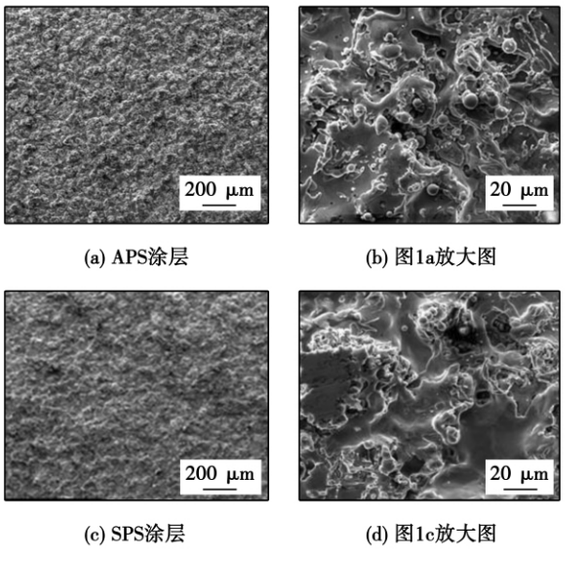

(a) APS涂层 (b) 图1a放大图

(c) SPS涂层 (d) 图1c放大图

图 1 喷涂态 NiCrCoAlY 涂层表面形貌

Fig. 1 Surface morphology of as-sprayed coatings

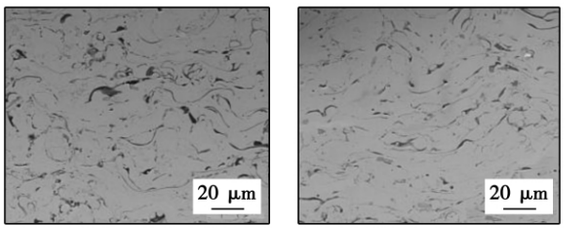

(a) APS涂层 (b) SPS涂层

图 2 APS 和 SPS 粘结层截面形貌

Fig. 2 SEM micrograph of APS and SPS bondcoat

2.2 粘结层孔隙率和显微硬度

表 1 为 SPS 和 APS 粘结层的孔隙率和显微硬度. 可以看出 SPS 粘结层孔隙率较 APS 粘结层低，显微硬度较 APS 粘结层高. 孔隙是由熔融或半熔融态的粒子互相搭接的间隙而形成的. 孔隙越多，涂层的致密性越低，从而使涂层的显微硬度下降.

表 1 SPS 和 APS 涂层的孔隙率和显微硬度

Table 1 Porosity and cross-sectional hardness of SPS and APS bondcoats

涂层	孔隙率 ϕ(%)	显微硬度(HV0.1)
SPS 粘结层	4.2	271.53
APS 粘结层	6.4	204.13

2.3 热障涂层结合强度

研究发现附加屏蔽气体后热障涂层的结合强度从 55.48 MPa 提高到 63.14 MPa. 其原因主要是 SPS 喷涂粘结层时粒子熔化情况较 APS 好，粒子和涂层的氧化程度较 APS 低，提高涂层的结合强度.

2.4 热障涂层抗高温氧化性能对比分析

2.4.1 氧化动力学分析

图 3 为 SPS 和 APS 粘结层及其 TBCs 在 1 080 ℃的氧化动力学曲线. SPS 和 APS 的粘结层和热障涂层的氧化动力学曲线基本上符合抛物线规律. 对比可以看出 SPS 粘结层和热障涂层的氧化增重较 APS 粘结层和热障涂层小，抗高温氧化性能更好.

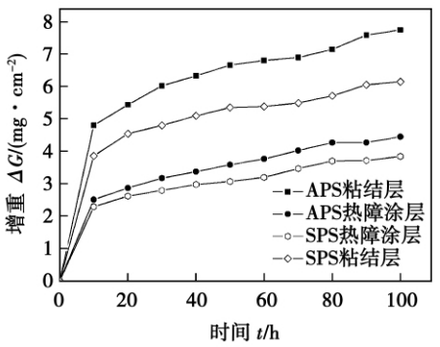

图 3 SPS 和 APS 粘结层及其 TBCs 在 1 080 ℃的氧化动力学曲线

Fig. 3 Comparison of oxidation kinetics at 1 080 ℃ for SPS and APS bond coating with and without ceramic top coating

2.4.2 粘结层氧化后表面产物特征

图 4 为 APS 和 SPS 粘结层在 1 080 ℃氧化 24 h 后表面形貌. 由图 4 可见 APS 粘结层表面很粗糙，在更高放大倍数下观察，其表面生成了许多瘤状氧化物. SPS 粘结层表面粗糙度小，除瘤状氧化物外还生成了细颗粒状氧化物. 分析(表 2)表明，瘤状氧化物主要为氧化铬，细颗粒状氧化物主要是 α-Al_2O_3，这是 α-Al_2O_3 的典型形貌[7]. XRD 分析(图 5a)也表明 SPS 粘结层 Al_2O_3 产物比 APS 粘结层表面更多一些.

2.4.3 热障涂层氧化后截面组织形貌

APS 和 SPS 热障涂层氧化前陶瓷层和粘结层结合良好，界面处无明显氧化物分布，陶瓷层表面凸凹不平且存在一定的孔隙和微裂纹. 高温氧化时，氧先进入陶瓷层中，再扩散到达粘结层. 陶瓷面层内互相连通的孔隙和裂纹易使氧向内扩散，另外即使陶瓷层是致密的，氧也能够达到很高的离子扩散速率[8]，从而使粘接层发生氧化.

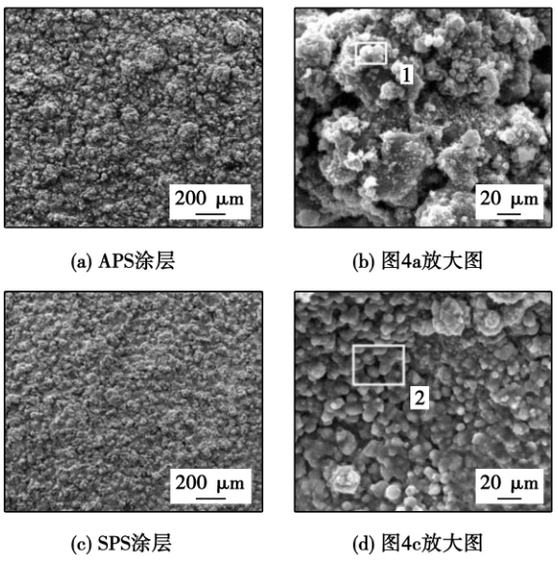

图 4　APS 和 SPS 粘结层氧化 24 h 后的表面形貌

Fig. 4　Surface morphology of APS coating and SPS bond coating after oxidation at 1 080 ℃ for 24 h

表 2　图 4 中各 EDS 选区元素组成(质量分数,%)

Table 2　EDS analysis results of selected area of Fig. 4

分析点	O	Cr	Ni	Al	Co	Y
1	50.95	31.70	17.35	—	—	—
2	31.21	10.22	22.70	31.77	0.58	3.52

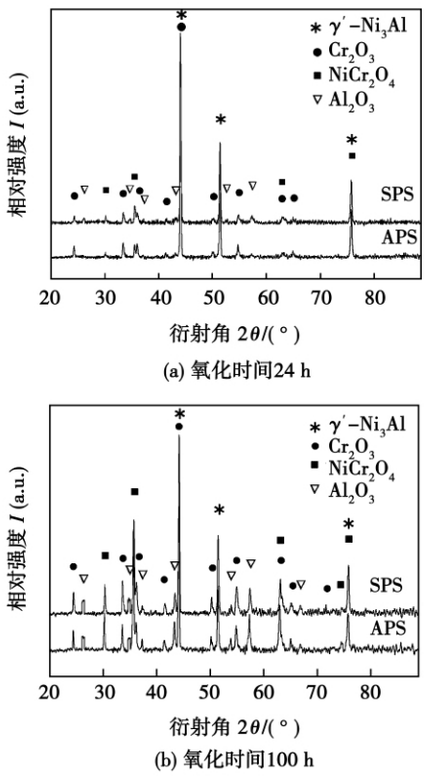

图 5　APS 和 SPS 粘结层氧化 24 h 和 100 h 后的 XRD 衍射图

Fig. 5　XRD patterns of APS and SPS bond coating after oxidation at 1 080 ℃ for 24 h and 100 h

对 SPS 和 APS 热障涂层氧化 10 h 和 24 h 后的截面观察发现,10 h 后 SPS 热障涂层在陶瓷层和粘结层界面生成了薄而连续的热生长氧化物(thermally grown oxide,TGO),APS 热障涂层虽也形成了 TGO,但 TGO 不连续. 当氧化时间增加到 24 h 后,两种热障涂层都形成了连续的 TGO,但 SPS 热障涂层比 APS 热障涂层生成的 TGO 更薄更致密. APS 热障涂层形成的 TGO 中 Al_2O_3 含量很低,主要由 Cr_2O_3 组成,而 SPS 热障涂层的 TGO 主要由 Al_2O_3 和 Cr_2O_3 组成(图 5a).

图 6 为 APS 和 SPS 热障涂层氧化 100 h 后的截面形貌. 可看出两种涂层都形成了连续的 TGO,但 APS 涂层的 TGO 更厚,且发生了严重的内氧化. 对图 6 中 A 点和 B 点的能谱分析(表 3)表明,TGO 成分主要为氧、铝、镍和铬. 结合 XRD 分析(图 5b)可以推断 TGO 的组成为 Al_2O_3,Cr_2O_3,$NiCr_2O_4$. 由于 Al 元素的化学活性高于 Cr 元素和 Ni 元素,因此最初生成的氧化物主要由 Al_2O_3 组成. 随高温氧化的不断进行,粘结层中的 Al 元素逐渐贫化. 当粘结层不能再提供全部生成 Al_2O_3 膜所需的 Al 元素量时,粘结层中的 Ni 元素和 Cr 元素就会大量参与氧化,形成 Ni 元素、Cr 元素的氧化物. 这种氧化物具有尖晶石结构,能产生较大的应力,使陶瓷层内部的裂纹相互连接,形成陶瓷层与粘接层界面方向的横向裂纹,裂纹扩展最终导致陶瓷层的脱落和整个热障涂层的失效(图 6a). 因 TGO 在界面处呈非均匀性生长,厚度起伏较大,直接测量比较困难,所以采用 Matlab 图像处理软件测量 TGO 层的面积,再除以

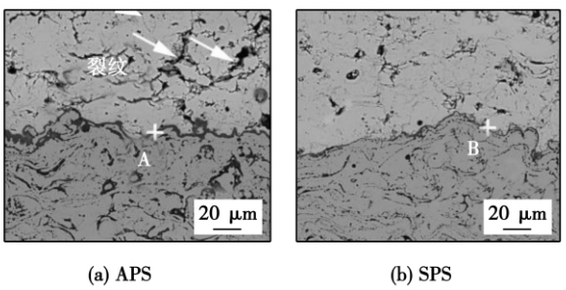

图 6　APS 和 SPS 热障涂层氧化 100 h 后截面形貌

Fig. 6　Cross-sectional SEM micrographs of TBCs after oxidation at 1 080 ℃ for 100 h

表 3　图 6 中 A,B 点成分的 EDS 分析结果(质量分数,%)

Table 3　Elements compositions of point A and B shown on Fig. 6

分析点	O	Cr	Ni	Al	Co
A	66.83	29.28	1.82	2.07	—
B	64.73	25.77	4.97	3.84	0.27

TGO层的长度，得到TGO层的平均厚度. 图7为两种热障涂层TGO层厚度与氧化时间的关系曲线. 可见SPS涂层TGO层的厚度增长速度小于APS涂层. 经高温氧化100 h后APS和SPS热障涂层的TGO层厚度平均值分别约为4.02 μm和2.62 μm. TGO的形成一方面对保护基体免受高温燃气腐蚀有利，另一方面当TGO达到一定厚度时累积的压应力会使涂层发生层离进而剥落.

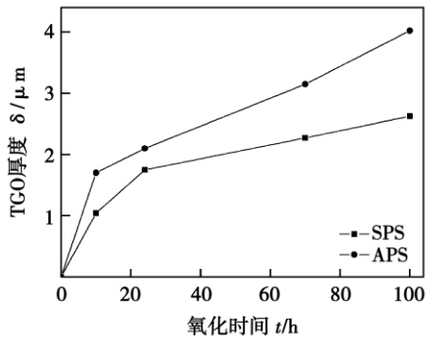

图7 热障涂层的氧化层厚度与时间的关系

Fig. 7 δ-t curves of TGO developed at APS coating and SPS coating

早期研究人员认为TBCs失效主要是由于陶瓷涂层是多孔性介质，强度低，在温度和外载荷的交互作用下容易发生断裂、脱落. 另外，由于涂层与基体的线膨胀系数和组织结构等的差别，容易产生应力集中使涂层脱落. 近年来，随着人们对热障涂层失效机理研究的深入，已经认识到TGO是造成热障涂层失效不可忽视的重要因素. 当热障涂层长期处于高温氧化气氛中时，陶瓷面层与粘结层界面在热、动力学条件驱动下形成TGO，并不断向内侧生长、加厚，并产生较大的应力. 当应力超过临界值时就会导致氧化膜破裂，并最终导致了TBCs的失效. 因此，延缓TGO的生长是改善TBCs抗高温氧化性能，延长使用寿命的重要途径之一.

铝对热障涂层的TGO的形成和耐高温氧化性能有重要的影响. NiCrCoAlY粉中铝含量本身就比较少，又由于APS喷涂时粒子和涂层的氧化比较严重，涂层中铝的含量进一步降低，这对Al_2O_3氧化膜的早期形成造成一定的影响，使TGO在高温环境中增厚速度加快，从而影响热障涂层的抗氧化性能. 而SPS喷涂时周围空气的卷入少，粒子和涂层氧化少，涂层氧化物夹杂少，粒子熔化充分，涂层致密，Al元素含量相对较高，涂层可以在高温氧化的早期形成比较致密的Al_2O_3氧化膜，使TGO增长速度减慢，因此有更好的抗高温氧化的性能.

3 结 论

(1) SPS喷涂比APS喷涂的粘结层的表面未熔或半熔粒子少，表面粗糙度小，涂层氧化物夹杂少，孔隙率低，硬度略高，TBCs结合强度高，粘结层和TBCs在1 080 ℃下具有更好的抗氧化性能.

(2) SPS比APS粘结层和TBCs在1 080 ℃的抗氧化性能优越的原因在于SPS喷涂时减少了周围空气的卷入和对焰流的扰动，粒子熔化充分，粒子和涂层氧化程度低，涂层致密且氧化物夹杂少，Al元素含量相对更高并有利于早期形成比较致密的Al_2O_3氧化膜，对粘结层有更好的保护效果，使TGO增厚速度减慢，陶瓷层与粘接层之间裂纹产生倾向降低，陶瓷层与粘接层结合状态保持得更好.

参考文献:

[1] Miller R A. Thermal barrier coatings for aircraft engines: history and directions [J]. Journal of Thermal Spray Technology, 1997, 6(1): 35 - 42.

[2] Fender E P, Fincke J, Spores R. Entrainment of cold gas into thermal plasma jets [J]. Plasma Chemistry and Plasma Process, 1991, 11(4): 529 - 543.

[3] Brandl W, Toma D, Kruger J, *et al*. The oxidation behaviour of HVOF thermal-sprayed MCrAlY coatings [J]. Surface and Coatings Technology, 1997, 94/95: 21 - 26.

[4] 管恒荣，李美姮，孙晓峰，等. 高温合金热障涂层的氧化和失效研究 [J]. 金属学报，2002(11): 1133 - 1140.
Guan Hengrong, Li Meiheng, Sun Xiaofeng, *et al*. Investigation on oxidation and failure of the thermal barrier coating deposited on superalloy [J]. Acta Metallrugica Sinica, 2002(11): 1133 - 1140.

[5] Menne U, Mohr A, Bammer M, *et. al*. Investigation of wear mechanisms of heat exchanger tubes under erosion conditions [C] // Thermal Spray: Research, Design and Applications. Las Vegas: ASM International, 1993: 277 - 282.

[6] Planche M P, Normand B, Liao H, *et al*. Oxidation control in atmospheric plasma spraying coating [J]. Surface and Coatings Technology, 2007, 202: 69 - 76.

[7] Doychak J, Smialek J L, Mitchell T E. Transient oxidation of single crystal NiAl [J]. Metallic Translation A, 1989, 20(3): 499 - 518.

[8] Fox A C, Clyne T W. Oxygen transport by gas permeation through the ziroconia topcoat in thermal barrier coating systems [C] // Proc. 15 th International Thermal Spray Conference, Nice. France, 1998: 1589 - 1594.

作者简介: 魏 琪，男，1953年出生，硕士，副教授. 主要从事焊接和表面工程方面的研究工作. 发表论文80余篇. Email: weiqi@bjut.edu.cn

metal; microstructure; brazing mechanism

Interfacial characteristics of welded joint between aluminum alloy and stainless steel by resistance spot welding QIU Ranfeng[1,2], YU Hua[1], SHI Hongxin[1], ZHAN Keke[1], TU Yimin[1], SATONAKA Shinobu[3] (1. School of Materials Science and Engineering, Henan University of Science and Technology, Luoyang 471003, China; 2. Henan Key Laboratory of Advanced Non-ferrous Metals, Luoyang 471003, China; 3. Graduate School of Science and Technology, Kumamoto University, Kurokami 2-39-1, Kumamoto 860-8555, Japan). p 37 - 40

Abstract: Aluminum alloy A5052 and stainless steel SUS304 were welded by resistance spot welding with a cover plate. The welding interface region of the joint was observed with electron microscopy, and the microstructure and distribution of the reaction products were analyzed as well. The results reveal that a serration reaction layer consisting of Fe_2Al_5 and $FeAl_3$ forms in the welding interface and the reaction layer thickness varies with the welding current and the position at the welding interface. Moreover, the reaction blocks in aluminum alloy near the welding interface were observed, which were estimated as a hexagonal AlFeCr having $a = 2.451$ nm and $c = 0.758$ nm based on analysis of selected area electron diffraction patterns.

Key words: aluminum alloy; stainless steel; resistance spot welding; interface reaction layer

Study on cold metal transfer welded lap joints of Mg/Al dissimilar metals SHANG Jing[1], WANG Kehong[1], TIAN Hongjun[2], ZHOU Qi[1], LI Guangle[1] (1. School of Material Science and Engineering, Nanjing University of Science and Technology, Nanjing 210094, China; 2. State-owned 5103 Factory, Nanzhao 474650, China). p 41 - 45

Abstract: AZ31B magnesium alloy and 6061 aluminum alloy were welded by cold metal transfer (CMT) welding method with pure copper (HS201) as the filler metal. Shear strength and micro-hardness of the lap joint were tested. The microstructure and fracture morphology of joint were studied by means of scanning electron microscope (SEM) and energy dispersive X-ray (EDX). The results showed that good weld with the highest shear bonding strength of 27.9MPa was obtained under the welding current of 109 A, welding voltage of 10.9 V, wire feed speed of 4.9 mm/s, welding speed of 0.45 m/min. Intermetallic compounds of Mg_2Cu and $MgCu_2$ were formed in the Mg-Cu side where was oxidized. Al-Cu-Mg ternary intermetallic compounds and Al_2Cu were formed on the Al-Cu side. Micro-hardness in both sides of fusion zone was suddenly increased due to intermetallic compounds. Maximum micro-hardness of Al-Cu side and Mg-Cu side were 242 HV and 347 HV respectively. The fracture occurred in the fusion zone of Mg side, and fracture nature was brittle fracture. Oxidation in the welding process and plenty of intermetallic compounds distributed continuously in the fusion zone, and resulted in the fracture.

Key words: cold metal transfer welding; aluminum alloy; magnesium alloy; dissimilar metals welding; intermetallic compounds

Preparation and properties of composite ceramic coating on AZ31B alloy by thermo-chemical reaction spraying MA Zhuang, ZOU Jifeng, WANG Wei, LI Zhichao (Institute of Materials Processing and Surface Technology, Liaoning Technical University, Fuxin 123000, China). p 46 - 50

Abstract: The spraying composite powder was prepared by mechanical ball milling and polyvinyl alcohol (PVA) granulation. Al_2O_3-based composite ceramic coating was prepared on the surface of magnesium alloy AZ31B by thermo-chemical reaction spraying. XRD and SEM were used to analyze the composition and morphology of the spraying composite powder and composite ceramic coating. The thermal shock, compactness, microhardness and wear properties of the composite ceramic coating were investigated respectively. The results showed that chemical reaction had happened in composite powder after 12 hours ball milling and globular structure coated each other was formed after granulation. Thermo-chemical reaction was carried out in the process of preparing coatings. New phase such as $Al_{3.21}Si_{0.47}$, $MgAl_2O_4$ and $Mg_{3.5}Al_9Si_{1.5}O_{20}$ were found in the coating. The melting rate of composite ceramic coating was high and the combination of the coating and matrix was good. Mg element took place remarkable diffusion in the interface of composite coating. The thermal-shock times of this coating was 40, the porosity was 15.1% and the maximum microhardness value reached $HV_{0.1}$ 1016. The thermal shock, compactness, microhardness and wear properties of this coating was significantly better than the ones with common spraying coating.

Key words: magnesium alloy; thermo-chemical reaction spraying; ceramic coating; performance

Influence of gas shroud on property of plasma sprayed thermal barrier coating WEI Qi, LI Hui, LI Hong, ZHANG Linwei (College of Materials Science and Engineering, Beijing University of Technology, Beijing 100124, China). p 51 - 54

Abstract: The comparative study were carried out on the microstructure as well as the properties of the coating prepared by atmospheric plasma spraying and shroud plasma spraying. The results showed that, compared to the conventional atmospheric plasma sprayed (APS) coating, the shroud plasma sprayed (SPS) coating contained less unmelted or partially melted particles and oxide content, and porosity was lower. The SPS coating presented superior oxidation resistance at 1 080 ℃ than the APS one. The reason owed to the mitigation of the involvement of the surrounding air that caused turbulent of the plasma, consequently, the particles were more fully melted and less oxide formed in the coating. The finally deposited SPS coating was denser and contained more Al element, which induced the formation of compact Al_2O_3 layer at the early stage of oxidation. This compact Al_2O_3 layer would slow down the thickening rate of thermally grown oxide (TGO) that provides better resistance to the bond layer, therefore the SPS coating presents higher resistance to high temperature oxidation.

Key words: plasma spray; thermal barrier coating; oxidation resistance

Influence of welding sequence on welding residual stress distribution in thick plate joint DENG Dean[1], SHOICHI Kiyoshima[2] (1. College of Materials Science and Engineering, Chongqing University, Chongqing 400045, China; 2. Research Center of Computational Mechanics, Inc., Tokyo 142-0041, Japan). p 55 - 58

Abstract: Features of welding residual stress distribution in an austenitic stainless steel thick plate joint were investigated by means of experiment and numerical simulation technology.